Reconstruction and Evaluation of a Single-scanning LiDAR-based wind Field Measurements using LES

Masakage Taguchi[1], Jay Prakash Goit[2], and Takatsugu Kameda[2]

[1]Graduate School of System Engineering, Kindai University, Higashi-Hiroshima, Hiroshima 739-2116, Japan
[2]Department of Mechanical Engineering, Kindai University, Higashi-Hiroshima, Hiroshima 739-2116, Japan

Correspondence: Jay Prakash Goit (jay.goit@hiro.kindai.ac.jp)

Abstract. Doppler LiDARs are considered as promising alternative to meteorological masts for wind resource assessments for wind energy application. The current study models a single scanning LiDAR-based wind field measurements in the LES and quantify the effect of scan parameters, i.e, measurement range, azimuth and elevation angles and wind direction on the accuracy of two-parameter velocity volume processing (VVP) method for computing velocity vectors from radial wind speeds. The mean wind speeds computed from LiDAR measurements show good agreement with the original LES data. The error increases with the measurement range, but it decreases with azimuth range, with $\theta_{\text{range}} = 60°$ giving the most accurate mean wind speeds among the three azimuth range considered in this study. The wind direction did not particularly effect the accuracy of the mean wind speed estimation, though larger difference between wind direction and scan direction results in increased variation in the VVP fitting. The effect of elevation angle is investigated with lower elevation angle scan of $3.4°$. Although stronger shear near the ground led to larger difference between the LiDAR and LES data, for higher points the effect of vertical shear on mean wind speeds is not significant. In terms of turbulence intensities, the two-parameter VVP significantly underestimates their values for all the case considered in this study. This is because a significant fraction of the fluctuating components is filtered out while fitting the data over the scan arc. The study therefore, proposes an improvement to the conventional VVP method, based on the Reynolds decomposition of wind speed components. Turbulence intensities estimated using this method show higher degree of variation, though the accuracy improved with increasing azimuth range.

1 Introduction

Doppler LiDARs have received significant attention as alternative to meteorological masts (met-masts) for wind resource assessments at potential wind energy development sites. They are considered particularly promising for offshore sites, where installation of tall met-masts can be significantly expensive and challenging compared to the onshore met-masts. Commercially available Doppler LiDARs for wind measurements are of two types, namely 1. profiling LiDARs which measure vertical profiles of wind speeds, directions and 2. scanning LiDARs which can perform volumetric scan for the given azimuth and elevation angle ranges. For offshore deployment, profiling LiDARs installed on the floating buoys are considered as economic alternative to the conventional met-masts (Viselli et al., 2019). Single or dual scanning LiDARs on the other hand are being deployed at coasts to perform measurement at near-shore offshore sites (Shimada et al., 2020, 2022). However, LiDARs can

25 only measure wind speed components along the beam direction, commonly known as radial wind speed (u_r). Various methods, which mainly depend upon the type of scan, are employed to estimate velocity vectors ($\mathbf{V}$) from the measured radial wind speeds (Holleman, 2005; Easterbrook, 1975; Sathe and Mann, 2013). One of the most common methods used to compute velocity vectors from a single scanning LiDAR is called velocity volume processing (VVP), in which wind speed from volumetric scan data is estimated using multivariant regression analysis (Easterbrook, 1975). However, further investigation is necessary to

30 evaluate the accuracy of the VVP-based method and the parameters that can influence the computed wind speeds. In particular, turbulence intensity computed using this method is believed to be less reliable. In the current study, we reconstruct wind field measurement of a single scanning LiDAR in large-eddy simulations (LES), and perform thorough evaluation of mean wind speeds and turbulence intensities obtained from the VVP.

One of the most commonly employed scan mode of a scanning LiDAR is plan-position indicator (PPI) scan, in which the

35 LiDAR beam sweeps over a range of azimuth angle (typically 30 to 60°), for the fixed elevation angle such that the measurements are taken on an arc-shaped trajectories (Barthelmie et al., 2016). As stated earlier, VVP method originally proposed by Easterbrook (1975) for wind radar application and further modified in other investigations (Frehlich, 2013; Shenghui et al., 2014) is used to retrieve velocity vectors from the measured radial wind speeds. In the most general VVP, the wind speed is assumed to vary linearly inside the scan volume, thus resulting in 12 fitting parameters(Waldteufel and Corbin, 1978). However,

40 in wind energy application two variant VVP (discussed in Section 2) is more commonly used. In this regard, Courtney et al. (2014) tested several scanning patterns at the test site of Danish Technical University and concluded that the azimuth range of 45° and scan rate of 3°/s performed the best. Coutts et al. (2015) also performed similar validation campaigns by comparing the LiDAR measurements against those of met-mast positioned 1.8 km away. Shimada et al. (2020) investigated the accuracy of the two variant VVP at the coastal site in Japan. They performed measurement with nine different scan settings and found that

45 for offshore site with negligibly small vertical wind speed component, the method could accurately measure mean wind speeds and directions. However, the variation in turbulence intensity was significant when compared against the sonic anemometer measurements.

An alternative to the VVP method is to align LiDAR scan along the mean wind direction or to measure wind direction using another device–e.g. sonic anemometer or wind vane installed on a met-mast–and assume that the direction is same at every

50 point on the scan surface. Similar methods were used to measure flow fields around wind turbines (Iungo and Porté-Agel, 2014; Goit et al., 2020). But recently, dual and triple scanning LiDAR-based measurements have gained more interest in wind energy community, as the method can be expected to give highly accurate wind speeds (Stawiarski et al., 2013). In their measurement campaign, Simon and Courtney (2016) showed that agreement between dual Doppler LiDAR and the reference cup anemometer measurement was excellent with error of less than 0.1% and extremely low scatter. Single LiDAR measurement

55 also showed good agreement with the cup anemometer data (0.2% error), though with a larger scatter. Newsom et al. (2015) compared the wind data retrieved from dual-Doppler LiDAR measurement against the measurement of sonic anemometer installed on the 60 m tall met-mast and reported the correlation coefficient of 0.97 for mean wind speed and difference of less than 0.1° for wind direction. In their validation campaign of dual scanning LiDAR, Shimada et al. (2022) reported that in addition to 10-min average wind speeds and directions, the system could also give turbulence intensity values comparable to

Table 1. Advantages and disadvantages of a single and multiple LiDARs.

Single LiDAR	Multiple LiDARs
1. Cheaper compared to multi-LiDAR measurements	1. Expensive-atleast twice for dual-LiDAR measurements.
2. Parameters influencing the measurement accuracy is not completely know.	2. Highly accurate wind speed measurement in possible.
3. Fewer constraints related to installation.	3. LiDARS have to be installed apart, so that they are at a certain angle (ideally 90°). Finding appropriate installation sites in complex terrain or coastal region can be challenging.
4. Data availability is comparatively higher. Distance from the measurement points and atmospheric conditions (aerosol concentration, presence of cloud, or mist layers) influence the availability	4. Data availability is lower. Data for wind directions perpendicular to the scan directions for either of the LiDARs have to be removed.
5. Velocity vectors can be measured along a line, thus resulting in more measurement points.	5. Measurements is only possible at a single target point.

those from cup anemometers. Although the studies have shown that multiple scanning LiDARS would certainly measure wind data accurately, its important drawback is that it will increase the cost of wind resource assessment at least by twice. For the offshore measurement, coastal terrain can impose limitations on the installation of LiDARs. For example, the LiDARs have to be installed few kilometer apart and scan direction of the either of the LiDARs should not be perpendicular to the dominant wind direction, so that higher data availability is maintained. Table 1 summarizes advantages and disadvantages of single and multiple LiDARs.

The above reviewed and other measurement campaigns are mostly validated against the single point data from met-masts, and are also influenced by environmental conditions such as lower aerosol density. Therefore, in order to quantify the accuracy of LiDAR measurements and VVP methods, it is necessary to simulate them using computational fluid dynamics (CFD) so they can be validated under the ideal condition. In this regards LES can become an important tool for LiDAR study, since it can simulate the atmospheric boundary layer (ABL) flow with high accuracy. Stawiarski et al. (2015) performed LES to simulate dual-Doppler LiDAR measurements and investigate whether the method can be used to detect and quantify coherent structures in the atmospheric surface layer. Rahlves et al. (2022) performed virtual Doppler LiDAR measurement in LES to investigate the effect of scan strategy on the measurement error of profiling LiDARs. LES has also been coupled with data assimilation technique to reconstruct ABL flow fields from a virtual LiDAR measurements (Bauweraerts and Meyers, 2021). More recently, Sanchez Gomez et al. (2022) also employed virtual LiDAR in LES to evaluated difficulties and uncertainties in measuring wind farm-induced blockage using scanning Doppler LiDAR.

However, as far as the authors are aware the VVP method has not been evaluated sufficiently, either through extensive measurement campaigns or numerical studies. The current study models single scanning LiDAR-based wind field measurements in the LES of ABL flow. One of the main objectives is to quantify the effect of the scan parameters, such as measurement range, azimuth and elevation angles, incoming wind direction on the mean wind speeds and turbulence intensities retrieved using the

VVP method. The study also proposes a modification to the existing method for computing turbulence statistics. This paper is further organized as follows: Section 2 describes the LES framework and and also provides details about the simulation cases considered in this study. The method for simulating a LiDAR in the computational environment and VVP-based wind speed retrieval technique is also described in this section. Section 3 evaluates wind speed retrieved using the two-parameter

85 VVP by comparing the results against the original LES data. Effect of the scan parameters are thoroughly discussed in this section. Since the turbulence statistic computed from the existing VVP method showed large uncertainty, Section 4 proposes a new method based on Reynolds decomposition of the radial wind speed for estimating turbulence intensities. Finally, Section 5 summarizes the main conclusions of this study.

2 Numerical method and case setup

90 Simulations of the ABL are performed using the open source CFD software OpenFOAM (ESI (2022)). We assume neutrally stratified ABL and model the flow fields using LES. The governing flow euations are the filtered Navier-Stokes equations given by:

$$\frac{\partial \tilde{u}_i}{\partial x_i} = 0 \tag{1}$$

$$\frac{\partial \tilde{u}_i}{\partial t} + \frac{\partial}{\partial x_j}(\tilde{u}_i \tilde{u}_j) = -\frac{1}{\rho}\frac{\partial \tilde{p}}{\partial x_i} + \nu \frac{\partial^2 \tilde{u}_i}{\partial x_j^2} + \frac{\partial \tau_{ij}}{\partial x_j} \tag{2}$$

95 where $\tilde{u}_i = [\tilde{u}_1, \tilde{u}_2, \tilde{u}_3]$ is the resolved velocity field corresponding streamwise, spanwise and verticalwise, $\tilde{p}$ is the instantaneous pressure field, ρ is air density, ν is kinematic viscosity, τ_{ij} is subgrid-scale stress. Tildes (˜) indicates spatial filter. The Wall-Adapting Local Eddy-Viscosity (WALE) model (Nicoud and Ducros, 1999) is used to model the effect of subgrid-scale stresses on the resolved flow fields. Figure 1 illustrates the schematic of the computation domain (for case 2 in Table 2). The boundary condition at the inflow plane is imposed using time varying flow field generated in a separate precursor simulation which is

100 discussed further below. The outlet boundary conditions are fixed value for the pressure and zero-gradient for the velocity fields. Slip condition and zero-gradient are applied at the top of the domain for velocity and pressure respectively. We have employed periodic boundary condition in the spanwise direction. Land and sea surfaces are modelled using the wall stress model (Mukha et al., 2019). To that end, surface roughness heights for land and sea surfaces are set to 0.2 m and 0.0002 m respectively.

105 The use of precursor data as inlet boundary condition has been well established in ABL simulations, and in particular simulations of large wind farms (Stevens et al., 2014; Munters et al., 2016). In the current study, precursor data is generated for the same domain and grid resolution as the actual simulations. Boundary conditions in the precursor simulations in both streamwise and spanwise directions are cyclic. This resulted in the regions with high speed and low speed streaks in the spanwise direction. In order to get rid of these streaks we impose spanwise shift to the precursor data (Munters et al., 2016).

110 However, instead of imposing a constant periodic shift, the study employs random shift size. The lower and upper limit of the shift size roughly correspond to the minimum($\approx$ 100 m) and maximum ($\approx$ 1000 m) width of the streak. Moreover, shift is performed every 100 s, so that its artificial effect on the generated wind field is minimized.
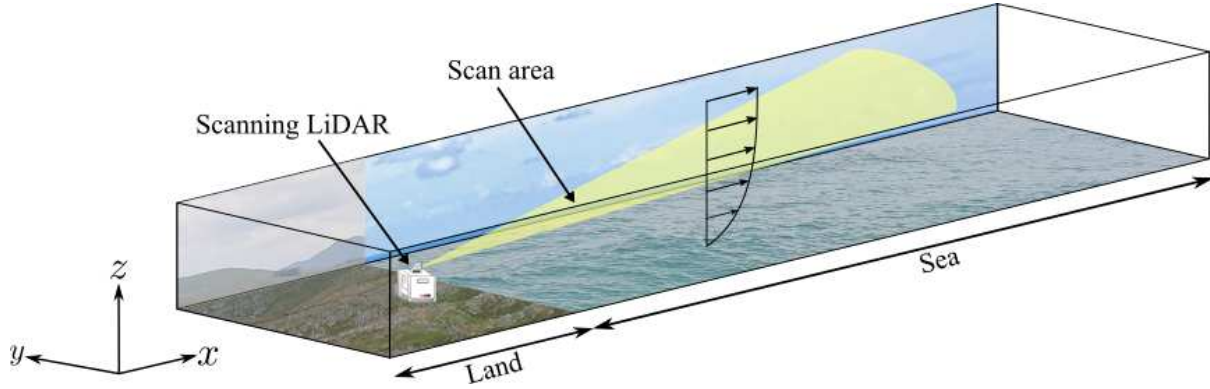
Figure 1. Schematic of the simulation domain and an example of a LiDAR scan.

Table 2. Summary of the simulation cases.

Case	Details	Surface roughness, z_0 (m)	Domain size $L_x \times L_y \times L_z$ (m^3)
1	Offshore only	0.0002	$10000 \times 1000 \times 4000$
2	Land-to-sea transition	Land: 0.2, Sea: 0.0002	$12000 \times 1000 \times 4000$ (land: 2000 m, sea: 8000 m)

2.1 Simulation cases

This study performs and analyses two simulations, details about which are summarized in Table 2. Case 1 simulates at-
mospheric boundary layer flow for offshore only condition, while case 2 considers land to sea transition. Case 1 can be
considered to simulate the measurement scenario with LiDAR installed on an offshore platform far from a coast or the
scenario when LiDAR is installed at the coast and wind blows from the direction of sea. Case 2 simulates for the mea-
surement with a LiDAR installed at the coast and wind blowing from land towards sea. Here, simulation domain size is
$L_x \times L_y \times L_z = 10000 \times 4000 \times 1000 \,\text{m}^3$ for case 1 and $L_x \times L_y \times L_z = 15000 \times 4000 \times 1000 \,\text{m}^3$ for case 2. Grid resolution
for all the cases are $\Delta x \times \Delta y \times \Delta z = 10 \times 8 \times 5 \,\text{m}^3$. Readers are referred to Goit and Önder (2022) for other details as well as
for the validation of the simulations.

2.2 Simulation of a scanning Doppler LiDAR in LES

In this study, scanning Doppler LiDAR-based measurement is reproduced in the LES environment. LiDAR can only measure
the wind speed component along the direction of emitted laser beam. This wind speed is known as radial wind speed (u_r) and
its relation to the velocity vector ($\mathbf{V} = [u_1, u_2, u_3]$) is shown schematically in Fig. 2. Since u_r is the projection of $\mathbf{V}$ along the
laser beam direction (r), it can be expressed as (see Koscielny et al. (1982)):

$$u_r = \mathbf{V} \cdot \mathbf{a_r}. \tag{3}$$
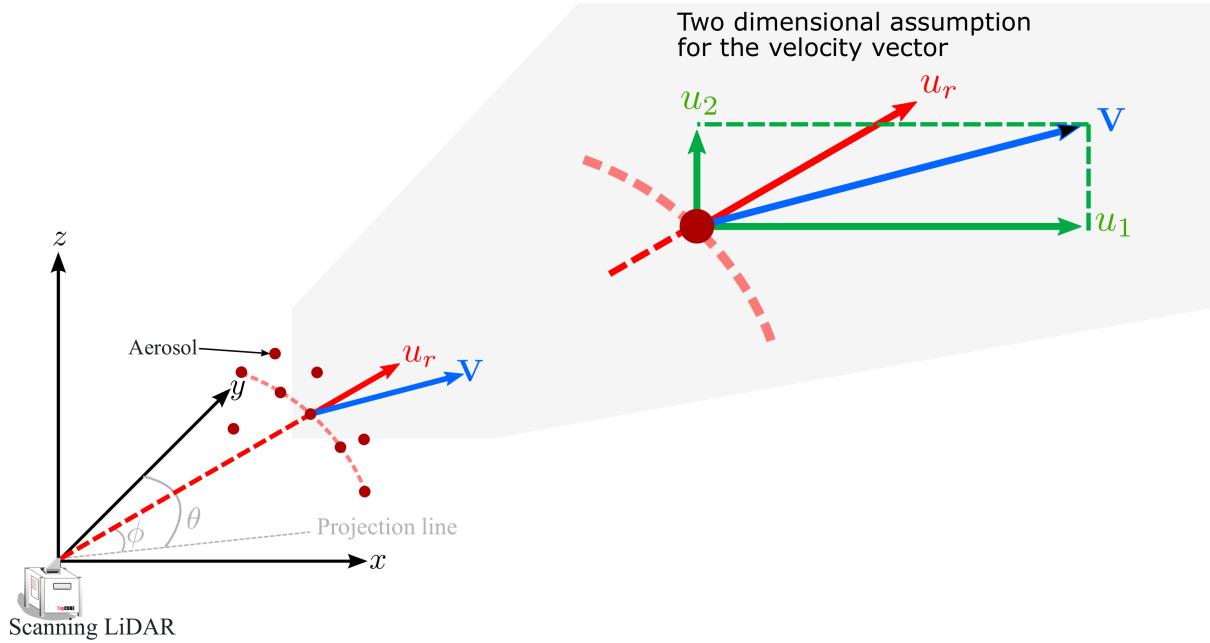
Figure 2. Schematic of the scanning Doppler LiDAR measurement and relation between radial wind speed (u_r) and velocity vector (**V**).

where $\mathbf{a_r}$ is the unit vector along r, i.e.,

$$\mathbf{a_r} = \sin\theta\cos\phi\,\mathbf{i} + \cos\theta\cos\phi\,\mathbf{j} + \cos\phi\,\mathbf{k}. \tag{4}$$

130 Here, θ is the azimuth angle and ϕ is the elevation angle. Since **V** values are known at all the grid points in the LES simulation, u_r can be computed from Eq. (3). To that end, LES data is first transformed into the polar coordinate system (r, θ, ϕ). Care is taken, such that radial, azimuth and elevation resolutions are similar to the commonly employed scan scenarios in actual measurement campaigns. However, the target points in the polar coordinate may not always have corresponding LES data points. Therefore, bilinear interpolation (see Appendix A) is applied to compute wind speeds on the polar coordinate system

135 of the LiDAR.

As stated earlier, VVP is one of the most common methods to compute velocity vector from the measured radial wind speeds. In this method, components of wind speed vector are assumed to vary linearly around their value $\mathbf{V_0} = [u_{1,0}, u_{2,0}, u_{3,0},]$ around the target point $r_0 = [x_{1,0}, x_{2,0}, x_{3,0}]$, which is usually selected to be at the center of the scan volume or the middle point on the scan arc. This can be approximated as (see Easterbrook (1975); Koscielny et al. (1982)):

140 $$u_i \quad \approx \quad u_{i,0} + \frac{\partial u_i}{\partial x_j}(x_j - x_{j,0}) \tag{5}$$

Substituting Eq. (5) into Eq. (3) gives:

$$u_r = u_{1,0}\sin\theta\cos\phi + u_{2,0}\cos\theta\cos\phi + u_{3,0}\cos\phi + \text{ derivative terms}. \tag{6}$$

Wind speed vectors can be computed from multivariant fitting of radial wind speeds to Eq.(6). Although this is the most general representation of the VVP method, with 11 parameters and vorticity terms requiring strong assumptions (Easterbrook, 1975),

145   the method is not considered practical. Instead, most of the recent studies assume spatial and temporal homogeneity during a short scan cycle and neglect derivative terms (Shimada et al., 2020). Furthermore, because the elevation angle is very small (5° or less) in most measurement campaigns, vertical component is considered negligibly small. Thus Eq. (6) simplifies to:

$$u_r = u_{1,0} \sin\theta \cos\phi + u_{2,0} \cos\theta \cos\phi. \tag{7}$$

Even though the expression is too simple to accurately represent wind field in the ABL, it is most commonly used method to

150   retrieve wind speed using a single scanning Doppler LiDAR. Therefore, this study also focuses on this two-parameter VVP method and attempts to evaluate their accuracy in-terms of mean wind speed and turbulence intensity measurements.

3   Two-parameter Velocity Volume Processing (VVP)

The study simulates scanning Doppler LiDAR-based measurements as discussed in section 2.2. Simulated radial wind speeds are then used to recompute velocity vectors using two-parameter VVP as described by Eq. (7).

155   Figure 3 shows a snapshot of instantaneous velocity fields in a vertical and a horizontal planes for the simulation case 1 ($z_0 = 0.0002$ m). Horizontal plane in the figure is taken at 120 m height as a representative of the hub height of many utility scale wind turbines. The virtual scanning LiDAR is placed at $x = 2$ km and $y = 2$ km of the domain. For case 1, it can be assumed that the LiDAR is installed on an offshore platform, while for case 2, it can be assumed to be on a platform at the coast and with the LiDAR head pointing towards the sea. The study follows meteorological coordinate system with the virtual

160   LiDAR at the origin. As a result, the scan azimuth angle $\theta = 0°$ is on the y-axis and it is positive in the clockwise direction. The scan interval in the azimuth direction is set to $d\theta = 3°$ and in the radial direction is set to $dr = 50$ m. Measurement range is $100 \leq r \leq 3000$ m. These scan parameters are defined based on most commonly employed values in actual field measurements.

3.1   Effect of azimuth angle and measurement range

This section discusses the effect of azimuth angle range (θ_{range}) and measurement range on the accuracy of the two-parameter

165   VVP. Table 3 lists the three scan scenarios employed for extracting radial wind speeds. In order to avoid the effect of the vertical wind shear as well as wind direction, elevation angle (ϕ) is set to 0° and the mean wind direction is 90° (i.e. westerly wind). In this way, centerline of the LiDAR scan aligns with the mean wind direction. Effect of wind direction and azimuth angle is discussed in the following subsections. Furthermore, the virtual LiDAR performs measurements at the height of 120 m which is more relevant for wind energy application.

170   Figure 4 shows the radial wind speed fields extracted from the LES for the three azimuth angle ranges listed in Table 3. It can be appreciated that the u_r fields show strong resemblance to actual LiDAR-based measurements (Banta et al., 2015; Zendehbad et al., 2015). Higher u_r values are observed on the center line of the azimuth range, i.e. $\theta = \pi/2$. This corresponds to the mean wind direction. u_r values decrease as azimuth angle moves away from $\theta = \pi/2$. This is more conspicuous in Fig. 4(c) of $\theta_{\text{range}} = 60°$.
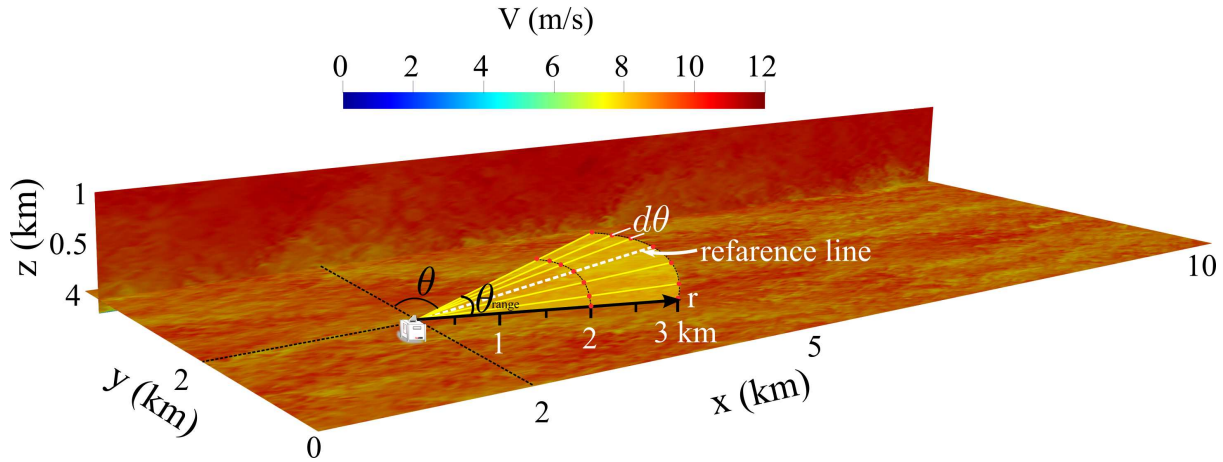
Figure 3. Snapshot of instantaneous velocity fields in a vertical and horizontal planes. Horizontal plane is taken at 120 m height.

Table 3. Summary of the scan scenarios for investigating the effect of azimuth range and distance.

θ_{range}	θ	$d\theta$	r	dr	ϕ	α
(°)	(°)	(°)	**(m)**	**(m)**	(°)	(°)
30	75 to 105	3	100 to 3000	50	0	90
45	66 to 111	3	100 to 3000	50	0	90
60	60 to 120	3	100 to 3000	50	0	90

θ_{range}: azimuth angle range; θ: azimuth angle; $d\theta$: Scan interval for azimuth angle range; r: measurement range; dr: Interval for measurement range; ϕ: elevation angle; α: wind direction.
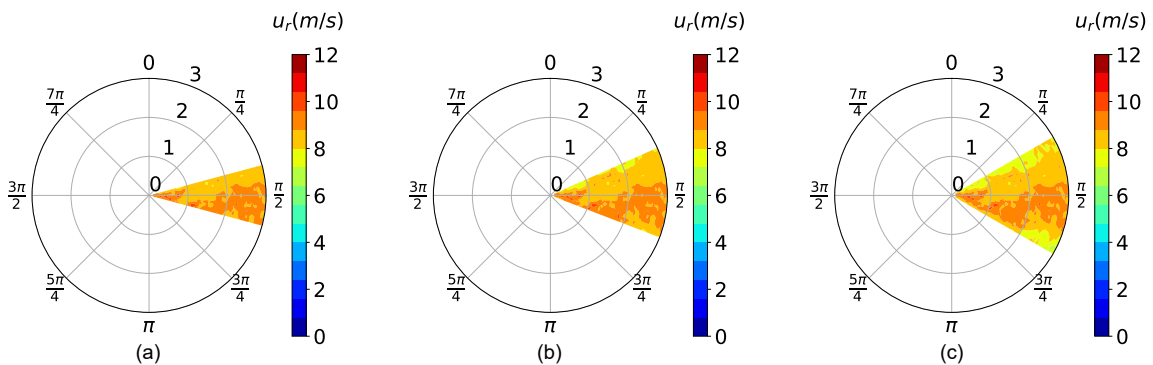
Figure 4. Radial wind speed fields extracted from the LES for different azimuth angle. (a) $\theta_{\text{range}} = 30°$, (b) $\theta_{\text{range}} = 45°$, (c) $\theta_{\text{range}} = 60°$.

175 Figure 5 compares the 10-minute average wind speed computed using the VVP method against those obtained from the original LES. Note that the LES wind speeds are extracted at the centerline of the azimuth range (i.e., $\theta = 90°$). It can be appreciated that there is a fairly good agreement between the LiDAR extratced wind speeds and the original LES data for both the cases. In order to quantify the error of wind speed reconstruction using the LiDAR data, we compute the relative error (ε)

$$\varepsilon \quad = \quad \frac{|\overline{u}_{\text{LES}} - \overline{u}_{\text{LiDAR}}|}{\overline{u}_{\text{LES}}} \times 100 \ [\%], \tag{8}$$

180 where $\overline{u}_{LES}$ is the actual wind speeds obtained from the LES and $\overline{u}_{\text{LiDAR}}$ is the wind speed computed from the virtual LiDAR measurement. Values of ε are shown in Fig. 5(c) and (d). The relative error is 0.173 to 2.68 % in the offshore-only case, and 0.467 to 7.98 % in the land-to-sea transition case. The larger error in the later case can be attributed to the higher turbulence–resulting in the greater inhomogeneity–in the flow which is generated over the land surface and persists several kilometers offshore (see Goit et al. (2022)).

185 Comparisons in Fig. 5 show that the error increase with the range. For example, for $\theta_{\text{range}} = 60°$ and in case 1, the error at the range $r = 500$ m is about 0.45% compared to about 1.0% at $r = 3000$ m. This is because the arc length increases with the range. For the longer arc length, 'spatial homogeneity' assumption of the VVP is not valid. For azimuth interval of $d\theta = 3°$ considered in this study, the radial wind speed data is extracted at an interval of 26 m at the range $r = 500$ m, while at the $r = 3000$ m, the interval increases to 157 m. Furthermore, for $\theta_{\text{range}} = 60°$, the arc length at $r = 500$ m is 524 m and at $r = 3000$ m is 3142
190 m. Consequently, the longer measurement range will result in the increase in the inhomogeneity on the arc. It is interesting to observe that in the case 2: land-to-sea transition, the error becomes smaller for $r \geq 2700$ m. For example, at $r = 2000$ m the error is $\varepsilon \approx 3\%$, compared to $\varepsilon \approx 1\%$ at $r = 3000$ m. This is because the land induced turbulence decreases with the offshore distance from the coast resulting in the more homogeneous flow field.

Figure 5(e), (f) shows the RMSE of the LiDAR data for the three θ_{range} and over the entire measurement range. RMSE is
195 given by:

$$\text{RMSE} = \sqrt{\frac{1}{N} \Sigma_{i=1}^{N} (\overline{u}_{\text{LiDAR}} - \overline{u}_{\text{LES}})^2} \tag{9}$$

where N is the number of data sample over the range $100 \leq r \leq 3000$ m. In terms of θ_{range}, the accuracy improves with larger azimuth range. With larger θ_{range}, equation for the VVP fitting, Eq. (6) can more accurately see the wind direction and compute the components of velocity vector. Furthermore, the number of data extracted from an arc for fitting also increases. Number of
200 data points for azimuth range of $30°$, $45°$ and $60°$ are 11, 16 and 21 respectively.

Although mean wind speed computed with a single scanning LiDAR two-parameter VVP is acceptable, accuracy in terms of turbulence intensity is not very promising. Figure 6 compares turbulence intensity computed using the VVP method against those obtained from the original LES. Turbulence intensity is defined as:

$$I = \frac{\sigma}{\overline{V}} \tag{10}$$

205 where σ is a standard deviation and $\overline{V}$ is a 10-minute average mean wind speed. Turbulence intensity computed from the VVP method decreases with the range. The best agreement can be observed at $r = 100$ m for all the cases. However, the
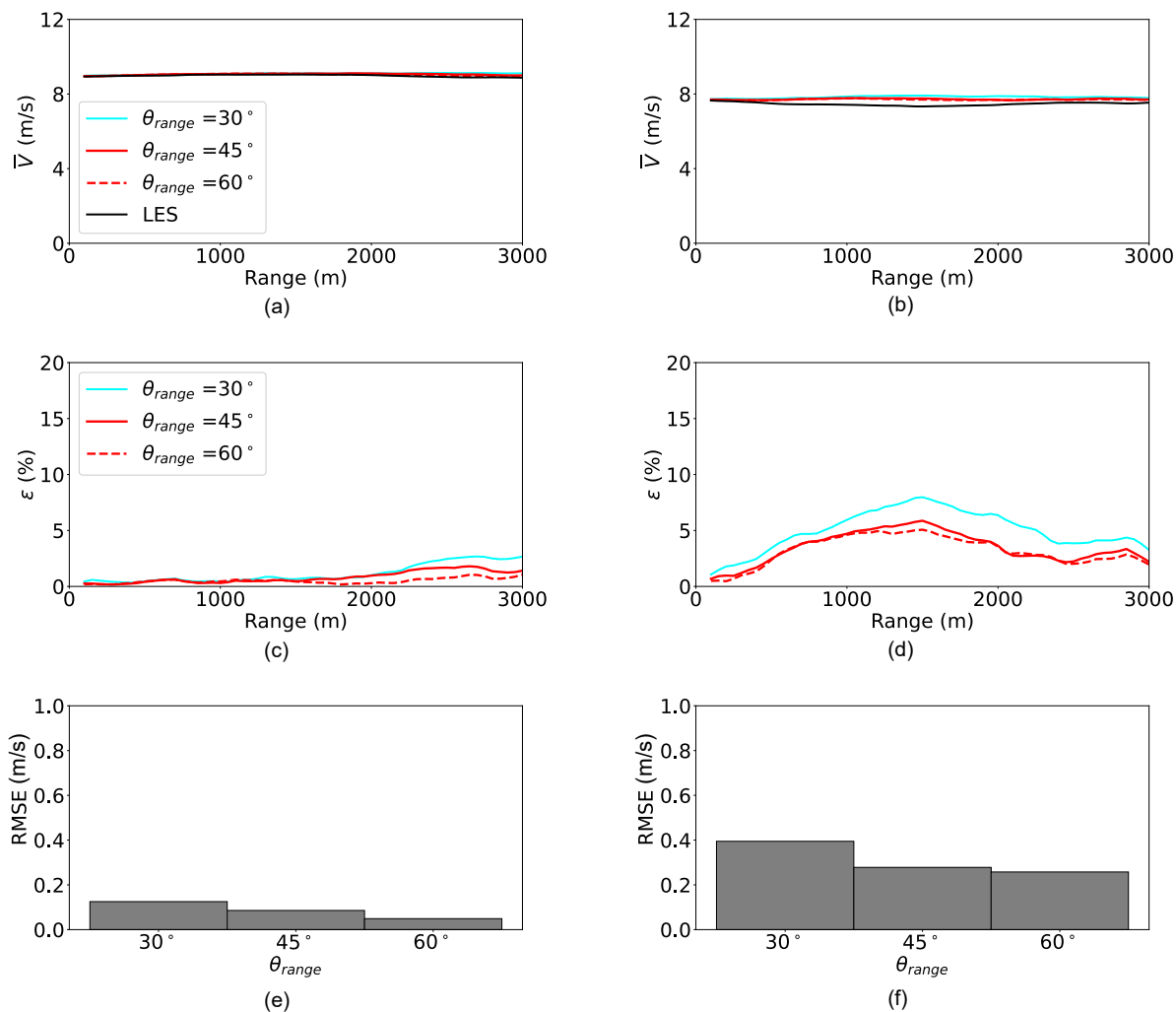
Figure 5. Comparison of 10-minute average wind speed computed using VVP against those obtained from the original LES simulations. (a), (b) show mean wind speeds as a function of range (r), (c), (d) show relative error, (e), (f) show RMSE of the comparison for each θ_{range}. (a), (c), (e): case 1 Offshore only; (b),(d), (f): case 2 Land-to-sea transition.
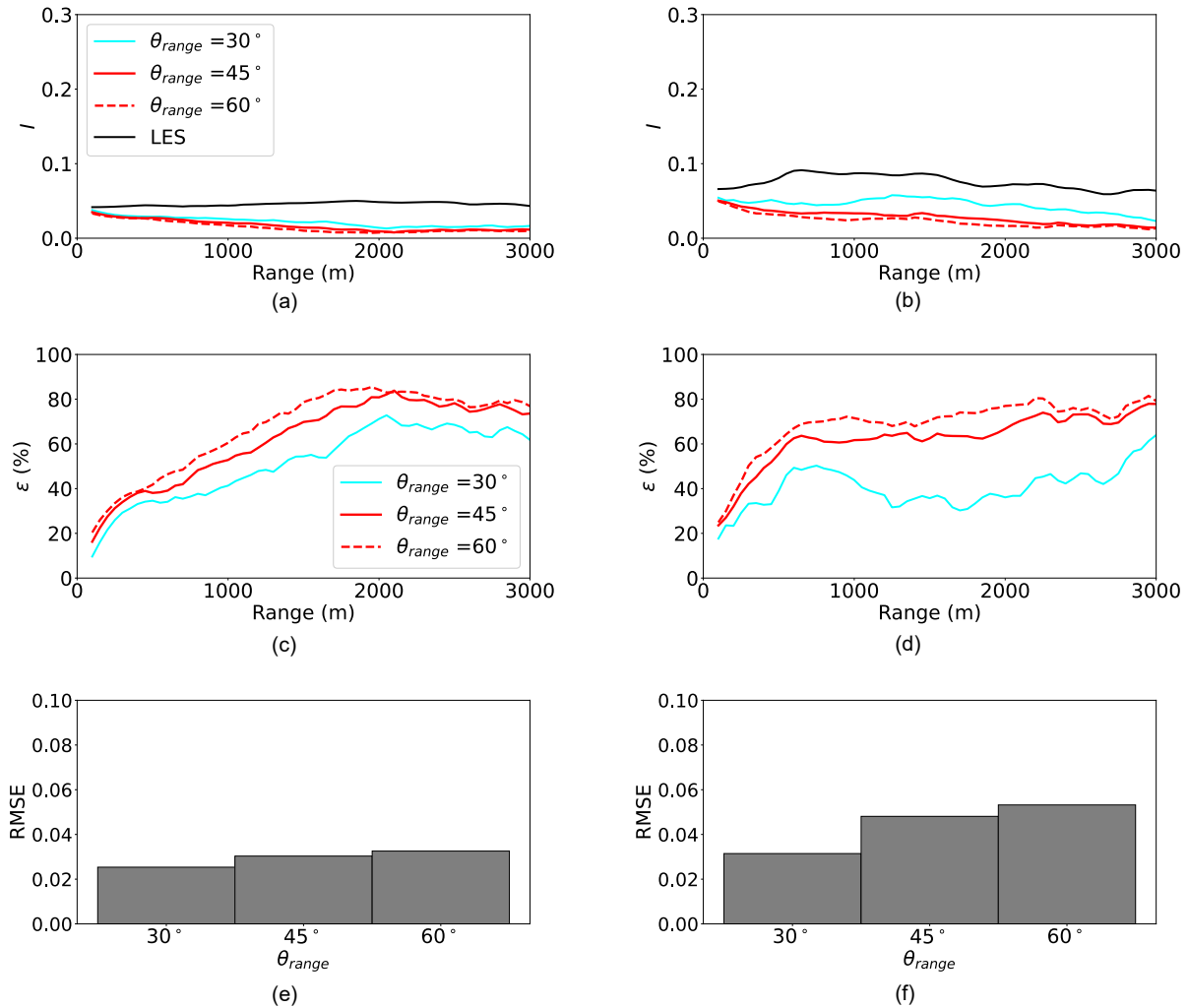
Figure 6. Comparison of turbulence intensity computed using VVP against those obtained from the original LES simulations. (a), (b) show turbulence intensities as a function of range (r), (c), (d) show relative error, (e), (f) show RMSE of the comparison for each θ_{range}. (a), (c), (e): case 1 Offshore only; (b), (d), (f): case 2 Land-to-sea transition.

VVP method significantly underestimates the turbulence intensities. For $\theta_{\text{range}} = 60°$, relative error $\varepsilon = 41.8\%$ at $r = 500$ m and 76.9% at $r = 3000$ m for case 1. Similarly, for case 2, $\varepsilon = 61.2\%$ and 79.1% at $r = 500$ m and 3000 m respectively. The errors increases significantly with the range, thus making the method less suitable for turbulence measurement. Figure 6 (e), (f) shows the RMSE of the LiDAR-estimated turbulence intensity for the three θ_{range} and over the entire measurement range. The RMSE increases with the azimuth range. Fitting to larger θ_{range}, filters out larger fraction of the fluctuating components from the computed wind speeds and consequently reducing the turbulence intensity values. This is further discussed in Section 3.4 below.

Table 4. Summary of the scan scenarios to investigate the effect of wind directions.

$\theta_{\mathbf{range}}$ (°)	θ (°)	$d\theta$ (°)	r (m)	dr (m)	ϕ (°)	α (°)
45	67.5 to 112.5	3	100 to 3000	50	0	90
45	21 to 66	3	100 to 3000	50	0	90
45	339 to 24	3	100 to 3000	50	0	90

3.2 Effect of wind direction

215   If α is a wind direction, then the horizontal wind speed components can be expressed as $u_{1,0} = V \sin \alpha$ and $u_{2,0} = V \cos \alpha$. Substituting theme into Eq. (7) gives

$$u_r = V \cos(\alpha - \theta) \cos \phi. \qquad (11)$$

It is clear from Eq.(11), that u_r is maximum when azimuth angle of the scan aligns with the wind direction and u_r decreases with increase in the difference between azimuth angle and wind direction and it becomes 0 m/s when $(\alpha - \theta) = 90°$. In an

220   actual field measurement, carrier-to-noise-ratio (CNR) decreases when u_r is close to 0 m/s, and therefore, the error in LiDAR measurements increases when $\alpha - \theta$ is around $90°$ (Goit et al., 2020). However, the effect of wind directions on the accuracy of two parameter VVP has not been addressed. In this section, the effect of wind direction is evaluated by varying azimuth angles relative to the wind direction. Table 4 lists the scan scenarios employed. Note that, case 1 offshore only is investigated here, so as to ensure that change in turbulence due to land-to-sea transitions and other effects are not introduced.

225   Figure 7 shows the radial wind speed fields extracted from the LES for three different azimuth angles relative to the mean wind direction($\alpha = 90°$). Compare to $67.5° \leq \theta \leq 112.5°$ whose centerline is aligned with the wind direction, the u_r value decreases for other two cases. In particular, at $\theta = 0°$ which corresponds to $\alpha - \theta = 90°$, the the radial wind speed is mostly 0 m/s. Note that u_r can also have negative values if $|\alpha - \theta| > 90°$ as can be observed in Fig. 7(c).

   Figure 8 compares 10-minute average wind speeds computed using VVP against those obtained from the original LES

230   simulations. Refer to Fig. 5(a) for $67.5° \leq \theta \leq 112.5°$ case. It can be appreciated that wind direction does not particularly affect the accuracy of the VVP. Provided that the noise level in the measured u_r is small and its availability is sufficiently high, the two parameter VVP employed in this study can accurately estimate mean wind speeds even if the difference between azimuth angle and wind direction is around $90°$. Note that, the error in Fig. 8(a) is comparatively larger for $r \geq 1700$ m. This is due to higher inhomogeneity in the original LES data for this scan area. The RMSE values, as shown in Fig. 8(c), are 0.1, 0.2

235   and 0.09 m/s for $|\alpha - \theta_c|$ of $0°$, $45°$ and $90°$ respectively. Here θ_c is the azimuth angle of the center line of a scan area. Larger RMSE value for $|\alpha - \theta_c| = 45°$ is the result of greater inhomogeneity for $r \geq 1700$ m for this scan direction.

   Figure 9 compares turbulence intensities computed using the VVP method against those obtained from the original LES. Unlike in Fig. 6(a), turbulence intensities computed from the VVP method do not decrease with the range. In fact in Fig. 9(b), turbulence intensities from the VVP method are even higher than that obtained from the LES. It was observed that larger
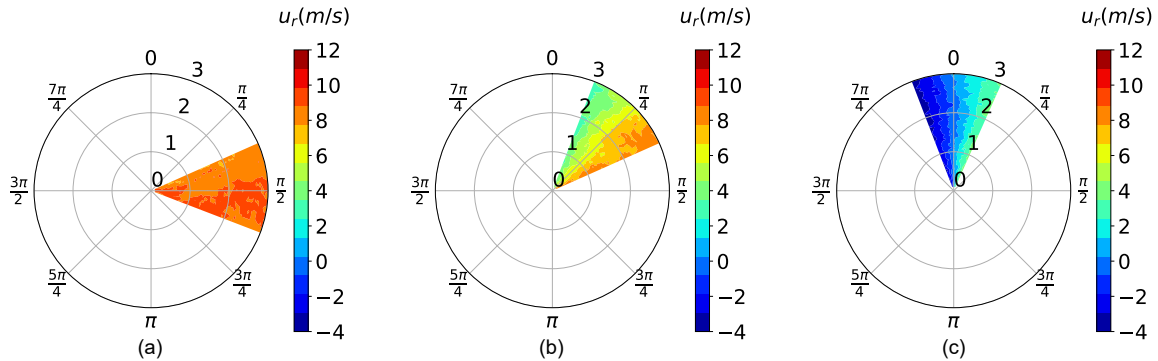
Figure 7. Radial wind speed fields extracted from the LES to investigate the effect of wind direction. Mean wind direction (α) is $270°$ for all three cases, whereas azimuth directions are (a) $67.5° \leq \theta \leq 112.5°$, (b) $21° \leq \theta \leq 66°$, (c) $339° \leq \theta \leq 24°$.

240 difference between wind direction and scan direction increased the variation in the VVP fitting. Therefore, even though the computed mean wind speeds are sufficiently accurate, higher variation results in larger turbulence intensity. The variation was the largest for the $|\alpha - \theta_c| = 90°$ case, which is why turbulence intensity is also the highest for this case. Although, RMSEs of the turbulence intensity are comparable to those in Fig. 6(e), and they improve for larger $|\alpha - \theta_c|$ values, this is just the result of increased variation during fitting. In reality turbulence estimation worsen for larger difference in the azimuth angle and wind

245 direction.

3.3 Effect of elevation angle

In the earlier sections the virtual LiDAR was assumed to be installed at the height of 120 m, so that the effect of vertical wind shear can be avoided from the VVP calculation. However, in reality LiDARs are generally installed on platforms few meters above the ground or above the sea surface. Therefore, measurements have to be performed at an elevation angle (ϕ) or a set of

250 elevation angles in order to obtain wind speeds at target heights. In this study, elevation angle is set to $\phi = 3.4°$, such that data is collected at the height of 120 m at $r = 2000$ m range from the LiDAR position. θ_{range} is set to $45°$, while all other parameters are same as earlier scan scenarios as summarised in Table 5.

Figure 10 compares 10-minute average wind speeds computed using the VVP from LiDAR scan at $\phi = 3.4°$ against those obtained from the original LES. Because of the elevation angle, the measurement height increases with range. This results in

255 increase in wind speed as a function of range. There is a fairly good agreement between the LiDAR extracted wind speeds and original LES data; in particular for case 1. This shows that the effect of vertical shear on the mean wind speed is not significant for offshore ABL. However, for case 2: land-to-sea transition, stronger shear near the ground leads to larger difference between the LiDAR and LES data for $r \leq 300$ m. Furthermore, we have only considered neutral ABL in the current study. Vertical shear may be important when thermal stratification is considered; in particular in convective ABL. The relative error $\varepsilon = 4.58\%$ at

260 $r = 500$ m and 0.492% at $r = 2000$ for case 1. As stated earlier $r = 2000$ m corresponds to the height of 120m. Similarly for
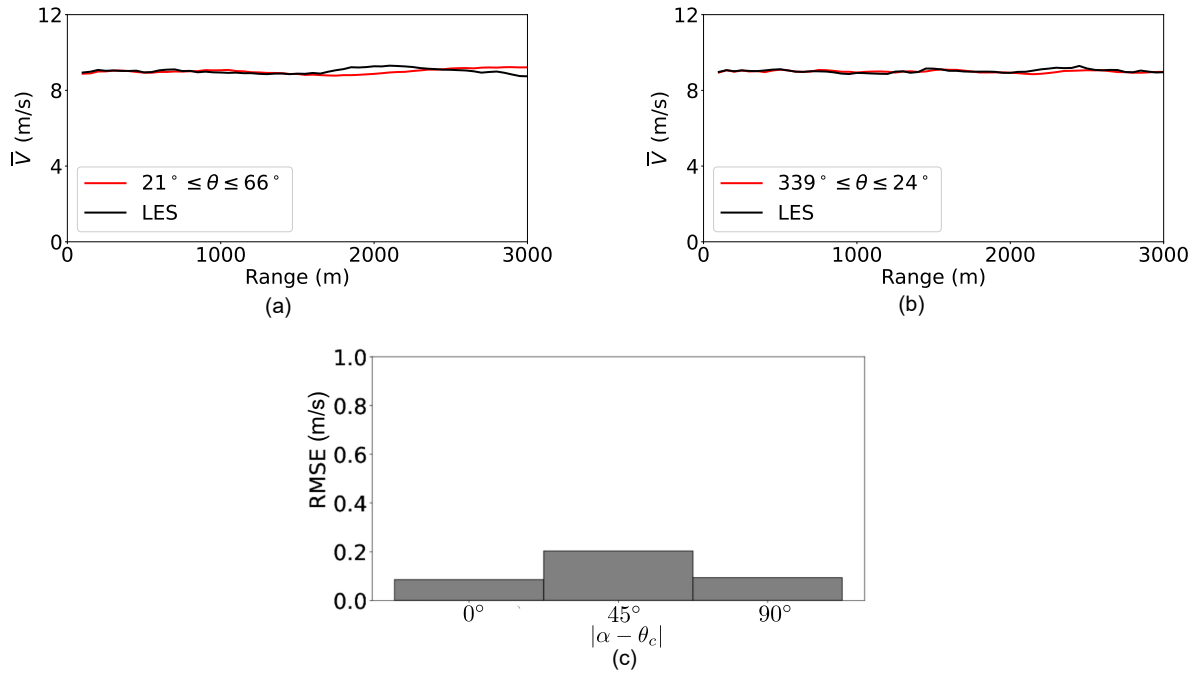
Figure 8. Comparison of 10-minute average wind speeds computed using VVP against those obtained from the original LES to evaluate the effect of wind direction. (a) $21° \leq \theta \leq 66°$, (b) $339° \leq \theta \leq 24°$ (c) RMSE of mean wind speed comparison.

case 2, errors are 4.84% and 4.05% at $r = 500$ m and 2000 m respectively. The errors are comparable to those of horizontal scans in Fig. 5.

Figure 11 evaluates the effect of elevation angle on turbulence intensity computed using the VVP method. The turbulence profiles show similar characteristics as those of horizontal scans in Fig. 6. Turbulence intensities computed from the VVP method show decreasing trend with the range. This is more pronounced in case 2 of land-to-sea transition. However, unlike the horizontal scan, in the near surface region, i.e., $r \leq 300$ m, the difference is larger. This is because, this region has a stronger shear which cannot be reproduced accurately using the two-parameter VVP. When we compare the two-parameter VVP against the general VVP equation Eq. (6), the former is missing term with vertical velocity component ($u_{3,0}$) and the terms with vertical derivative ($\partial u_i/\partial x_3$). In order to accommodate these terms, multi-layer volumetric scans have to be performed which will significantly reduce the sampling rate. In terms of relative errors, $\varepsilon = 52.4\%$ at $r = 500$ m and $\varepsilon = 78.4\%$ and $r = 2000$ m for case 1. For case 2, $\varepsilon = 49.7\%$ and 68.6% at $r = 500$ m and 2000 m respectively.

3.4 Discussion

It is clear from the analysis and comparisons above that mean wind speeds computed using the two-parameter VVP is fairly accurate. However, the method significantly underestimates the turbulence intensities. As discussed earlier, two-parameter VVP employs LiDAR-measured u_r over the scan arc for the given range and substitute them into Eq. (7) to obtain wind speed
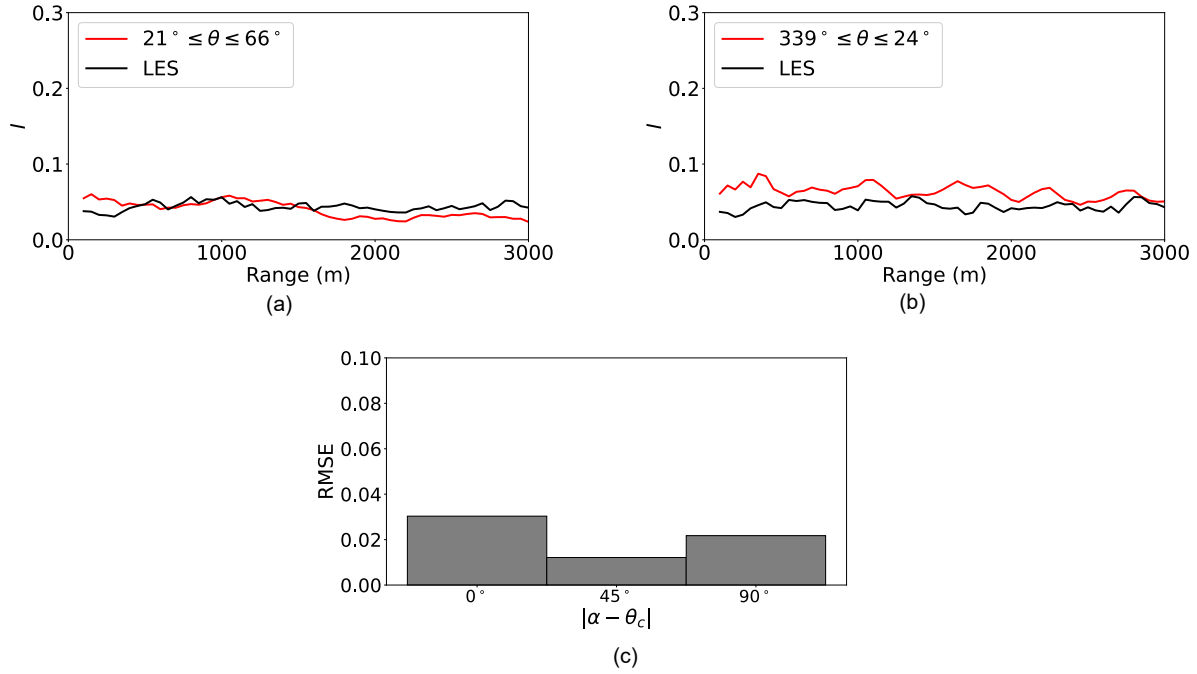
Figure 9. Comparison of turbulence intensities computed using VVP against those obtained from the original LES to evaluate the effect of wind direction. (a) $21° \leq \theta \leq 66°$, (b) $339° \leq \theta \leq 24°$ (c) RMSE of turbulence intensities comparison.

Table 5. Summary of the scan scenarios to investigate the effect of elevation angles.

θ_{range}	θ	$d\theta$	r	dr	ϕ	α
(°)	(°)	(°)	(m)	(m)	(°)	(°)
45	66 to 111	3	100 to 2000	50	3.4	0

vectors from the multivariant fitting. For example, for $\theta_{\text{range}} = 60°$, it uses u_r from 21 points over an arc. Fitting to the data over such large θ_{range} filters out significant fraction of fluctuation from the computed wind speeds and thus reducing the estimated turbulence intensity.

This is discussed using Fig. 12 which compares time series of instantaneous wind speeds computed using the VVP method against the original LES wind speeds (at the centerline of θ_{range}) and the LES wind speeds averaged over the scan arc ($\overline{V}_{\text{arc}}$). The last term, $\overline{V}_{\text{arc}}$ is defined as:

$$\overline{V}_{\text{arc}} = \frac{1}{N_\theta} \sum_{i=1}^{N_\theta} V_{\theta,i} \tag{12}$$

where N_θ is the number of data points on the scan arc for the given range and $V_{\theta,i}$ is the instantaneous wind speed for each azimuth angle. It is clear from the figure that compared to strongly fluctuating original LES wind speeds, VVP-estimated
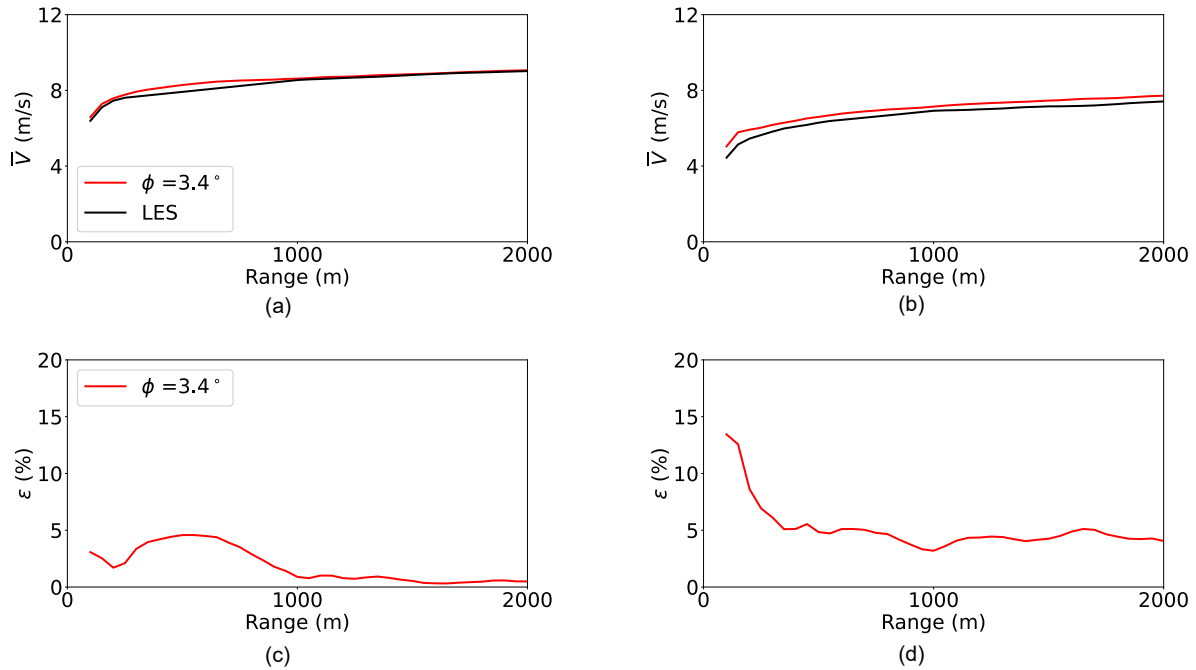
Figure 10. Comparison of 10-minute average wind speeds computed using VVP against those obtained from the original LES to evaluate the effect of elevation angle. (a), (b) show mean wind speeds as a function of range, (c), (d) show relative errors. (a), (c): case 1 Offshore only; (b), (d): case 2 Land-to-sea transition.

285 wind speeds are smoother. Furthermore, when observed at different ranges, the VVP-estimated wind speeds try to follow fluctuations with longer time scale at $r = 500$ m while, at $r = 2000$ or 3000 m, it is only able to estimate wind speed in the mean sense. This can be attributed to the size of the scan arc. For $\theta_{\text{range}} = 60°$, the scan arc length is 535 m at $r = 500$ m, and 3142 m at $r = 3000$ m. Even though the number of data points used are same for the given θ_{range}, the spacing between the data increases with range. Consequently, for a longer range, the VVP-method is not able to capture small scale fluctuations, resulting from spatial averaging during the fitting. Interestingly, VVP-estimated instantaneous wind speeds almost overlap with the arc-averaged wind speeds, i.e., $\overline{V}_{\text{arc}}$. This agreement corroborates, that while the two-parameter VVP method can accurately estimate wind speeds in the mean sense, it cannot provide accurate turbulence intensities.

The effect of scan arc length on the VVP-estimated wind speeds can also be observed in power spectral-densities (PSD) as shown in Fig. 13. Assuming that the VVP method is able to measure flow fields of the length scale ($\mathcal{L}$) similar to or larger than the size of the scan arc, and mean wind speed is a representative speed (u), then the corresponding characteristic time scale can be estimated from a simple dimensional analysis (see Tennekes and Lumley (1972)), i.e., $\mathcal{T} \sim \mathcal{L}/u$. This $\mathcal{T}$ for $r = 500$ m is 60 s and $r = 2000$ m is 250 s. The corresponding frequencies are 1.6×10^{-2} Hz and 4×10^{-3} Hz, respectively. In Fig. 13 (a) for $r = 500$ m, PSD of the VVP-estimated wind speeds shows similar trend to that of the LES wind speeds, though the
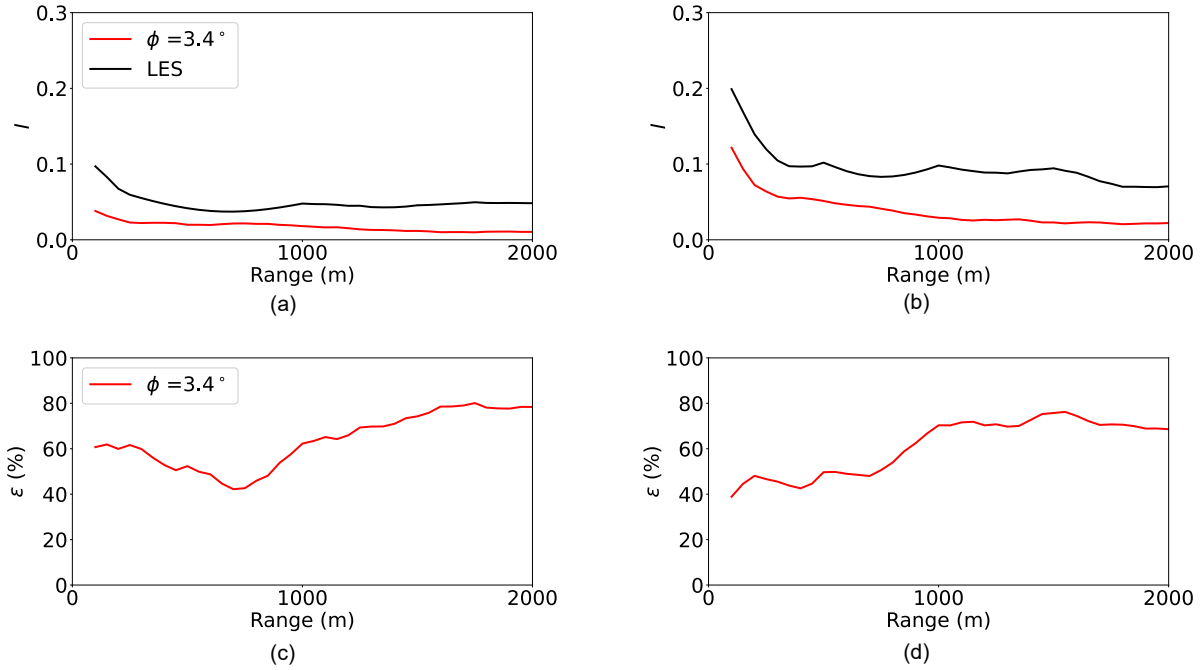
Figure 11. Comparison of turbulence intensities computed using VVP against those obtained from the original LES to evaluate the effect of elevation angle. (a), (b) show mean wind speeds as a function of range, (c), (d) show relative errors. (a), (c): case 1 Offshore only; (b), (d): case 2 Land-to-sea transition.

magnitude is smaller for higher frequencies. At $r = 2000$ m, the PSD from the VVP is smaller than that from the LES data for
300 all the frequencies.

4 Reynolds decomposition of u_r

This section presents a method that improves on the conventional VVP technique for computing turbulence intensity from a single LiDAR measured data. The method decomposes wind speeds into mean and fluctuation terms using Reynolds decomposition and develops a VVP equation for fitting the Reynolds stress terms. In this way, filtering effect due to the mean term 305 can be alleviated.

Reynolds decomposition of a radial wind speed and velocity vectors can be expressed as:

$$u_r = \overline{u}_r + u_r'$$
$$u_1 = \overline{u}_1 + u_1'$$
$$u_2 = \overline{u}_2 + u_2'. \tag{13}$$

Here, overline denotes time average and prime (′) denotes fluctuation. Substituting them into Eq. (7) gives:

$$(\overline{u}_r + u_r') = (\overline{u}_1 + u_1')\sin\theta + (\overline{u}_2 + u_2')\cos\theta. \tag{14}$$
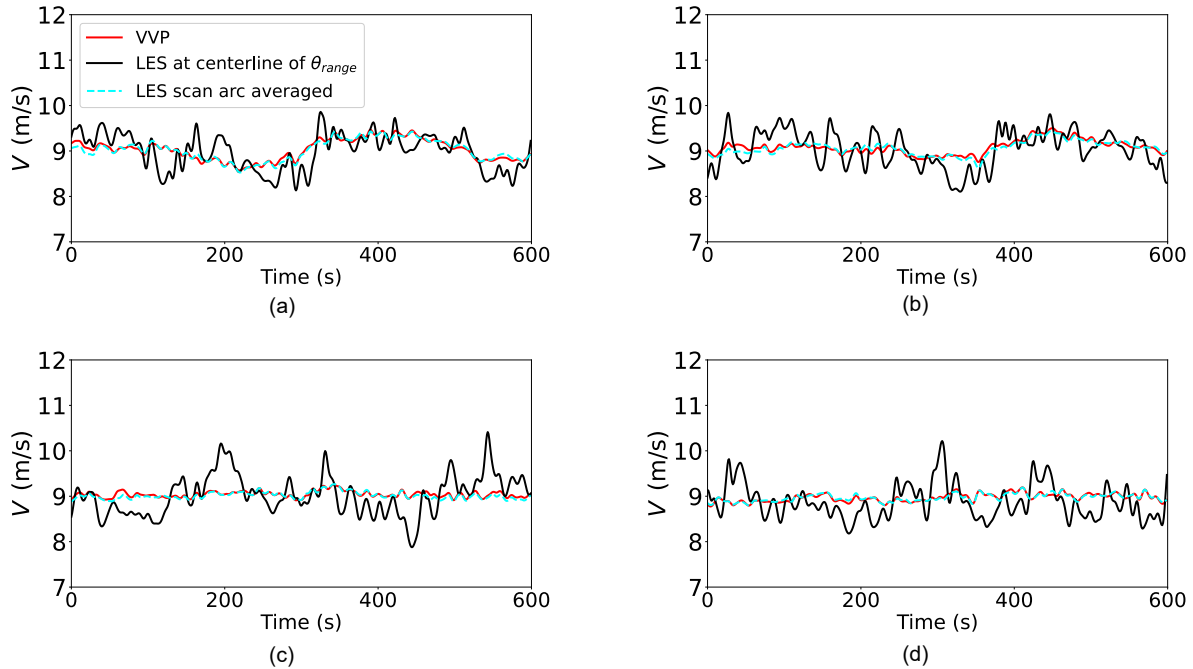
Figure 12. Time series of instantaneous wind speeds computed using VVP, wind speeds from original LES extracted from the centerline of the θ_{range} and LES wind speeds average over the scan arc for the given range. Results are shown for case 1: Offshore only with $\theta_{\mathrm{range}} = 60°$, and ranges are (a) 500 m, (b) 1000 m, (c) 2000 m, (d) 3000 m.
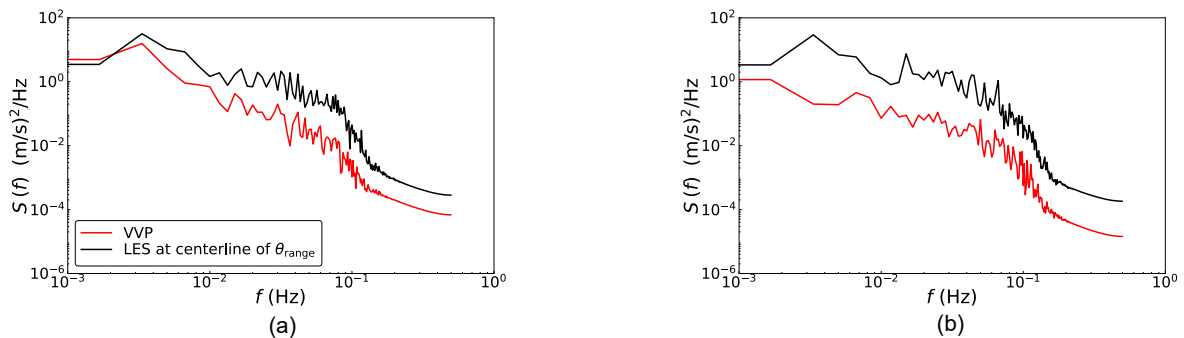
Figure 13. Power spectral densities of wind speeds computed using VVP and wind speeds from original LES extracted from the centerline of the θ_{range}. Results are shown for case 1: Offshore only with $\theta_{\mathrm{range}} = 60°$ and ranges are (a) 500 m, (b) 2000 m.

310   Next, taking square and time average on both sides yields:

$$\overline{u_r}^2 + \overline{u_r'^2} = \overline{u_1}^2 \sin^2\theta + 2\overline{u_1}\,\overline{u_2}\sin\theta\cos\theta + \overline{u_2}^2\cos^2\theta$$
$$+\overline{u_1'^2}\sin^2\theta + 2\overline{u_1'u_2'}\sin\theta\cos\theta + \overline{u_2'^2}\cos^2\theta \tag{15}$$

Similarly, the time average followed by square of Eq. (7) yields.

$$\overline{u_r}^2 = \overline{u_1}^2 \sin^2\theta + 2\overline{u_1}\,\overline{u_2}\sin\theta\cos\theta + \overline{u_2}^2\cos^2\theta \tag{16}$$

From Eq. (15) and (16) one can write:

315   $$\overline{u_r'^2} = \overline{u_1'^2}\sin^2\theta + 2\overline{u_1'u_2'}\sin\theta\cos\theta + \overline{u_2'^2}\cos^2\theta. \tag{17}$$

Here, $\overline{u_1'^2}$ and $\overline{u_2'^2}$ are normal stresses and $\overline{u_1'u_2'}$ is a shear stress. Turbulence intensity can be computed directly by fitting fluctuating components of radial wind speeds to Eq. (17).

Figure 14 compares turbulence intensity using the modified VVP method against those obtained from original LES. The estimated turbulence intensities show higher degree of variation and the values are even higher than the turbulence intensities
320   obtained directly from the LES. Nevertheless, the accuracy improves with increasing θ_{range}. This is atleast the case for $\theta_{\text{range}} = 60°$ in Fig. 14(a). In the land-to-sea transition case which has higher turbulence intensity the agreement is not very promising. The part of the reason may be the fewer number of u_r data used to fit to Eq. (17). Increasing the azimuth resolution (e.g. from $3°$ to $1°$) may improve the fitting. However, in actual field measurements that will reduce the sampling rate and may also reduce the data availability. It is interesting to observe that the RMSE decreases with θ_{range} for both the simulation cases.

325   ## 5   Conclusions

The current study has modelled a single scanning LiDAR-based wind field measurements in the LES of the ABL flow. Radial wind speeds measured by the LiDAR were used to recompute velocity vectors using the two-parameter VVP. Wind speeds retrieved in this way was then compared against the original LES data to quantify the effect of the scan parameters, such as measurement range, azimuth and elevation angles and incoming wind direction.
330   The mean wind speeds computed from LiDAR measurements showed good agreement with the original LES data. Even though the error increased with the range it was less than 3% for all the cases. In terms of θ_{range}, the accuracy improved with larger azimuth range, with $\theta_{\text{range}} = 60°$ giving the most accurate mean wind speeds among the three azimuth range considered in this study. The wind direction did not particularly effect the accuracy of the mean wind speeds. However, larger difference between wind direction and scan direction resulted in the increased variation in the VVP fitting. The effect of elevation angle
335   was investigated by performing scans for $\phi = 3.4°$. The effect of vertical shear on mean wind speeds was not significant for this elevation angle, though stronger shear near the ground lead to larger difference between the LiDAR and LES data. It should be noted that the vertical shear may become significant for onshore or convective ABLs, resulting in higher error due to elevation angle. This needs to be investigated in the future study.
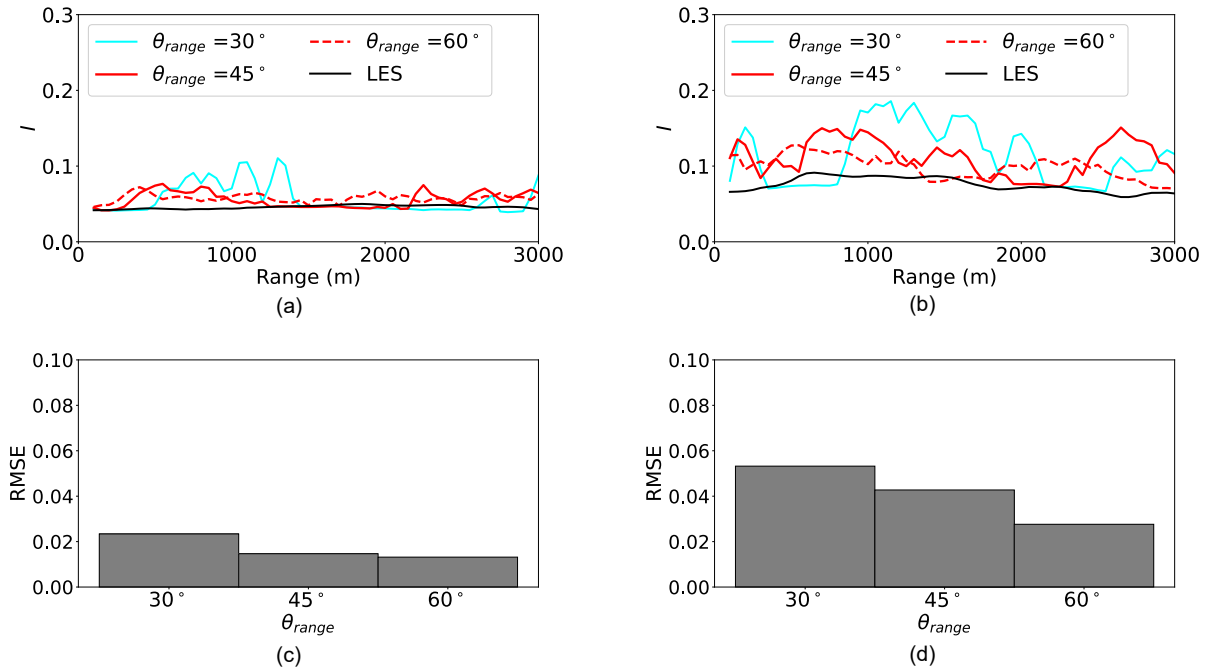
Figure 14. Turbulence intensity computed using Reynolds decomposition of the LiDAR-measured u_r. (a), (b) show turbulence intensities as a function of range (r). (c), (d) show RMSE of the comparison for each θ_{range}. (a), (c): case 1 Offshore only; (b), (d): case 2 Land-to-sea transition.

In terms of turbulence intensities, the two-parameter VVP significantly underestimated their values for all the case consid-
340 ered in this study. This was attributed to the filtering out of a fraction of fluctuation while fitting the data over the scan arc. The error increased significantly with the range. Therefore, we proposed a modification to the conventional VVP method based on the Reynolds decomposition of wind speed components. In the modified VVP, turbulence intensity was computed by fitting to the equation of fluctuating wind speeds. Turbulence intensity estimated in this way show higher degree of variation, though the accuracy improved with θ_{range}. The method for computing turbulence intensity with a single LiDAR requires further im-
345 provement. In the future work, we plan to minimize the variation resulting from fitting to the modified VVP equation. We also plan to investigate the effect of atmospheric stability, terrain feature and scan resolution parameters on the accuracy of LiDAR measurements.

Code and data availability. The study uses the open source CFD software OpenFOAM. The simulation cases can be reproduced based on discussion in section 2 and our earlier work https://doi.org/10.1063/5.0094476. The raw simulation data are available from the corresponding
350 author upon reasonable request.
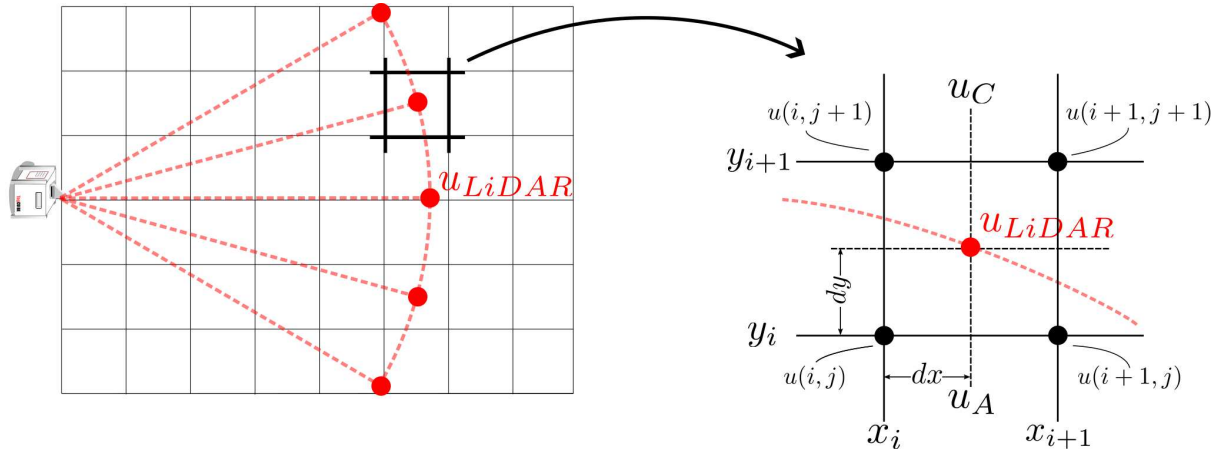
Figure A1. Bilinear interpolation scheme for estimating wind speeds on LiDAR grid points from original LES grid points. Dark lines represent LES grid and red lines represent LiDAR grid.

Appendix A: Extracting wind speeds on LiDAR coordinate system

LiDAR grid points which are defined on polar coordinate system, not necessarily have corresponding LES grid points defined on orthogonal coordinate system. We therefore employ bilinear interpolation to estimate wind speeds on LiDAR grid points. Figure A1 shows the schematic of the interpolation scheme for the two dimensional case.

355   Wind speeds at A and C can be interpolated from the data at four LES grid points:

$$u_A \quad = \frac{u(i+1,j) - u(i,j)}{x_{i+1} - x_i} \, dx + u(i,j) \tag{A1}$$

$$u_C \quad = \frac{(u(i+1,j+1) - u(i,j+1))}{(x_{i+1} - x_i)} \, dx + u(i,j+1) \tag{A2}$$

Velocity at the LiDAR grid point can be expressed in the form of u_A and u_C:

$$u_{\text{LiDAR}} = \frac{u_C - u_A}{y_{j+1} - y_j} \, dy + u_A. \tag{A3}$$

360   Next, substituting from Eq. (**??**) to Eq. (A3) and re-arranging the terms:

$$u_{\text{LiDAR}} = \quad \frac{u(i,j) - u(i+1,j) - u(i,j+1) + u(i+1,j+1)}{(x_{i+1} - x_i)(y_{j+1} - y_j)} \, dx \, dy$$
$$+ \frac{u(i+1,j) - u(i,j)}{x_{i+1} - x_i} \, dx + \frac{u(i,j+1) - u(i,j)}{y_{j+1} - y_j} \, dy + u(i,j) \tag{A4}$$

Eq. (A4) is used to compute wind speeds on LiDAR grid points. Similar expression can be used to estimate all three wind speed components. Interpolated wind speeds are used to compute u_r in Eq. (3) and the method is shown in Fig. A2.
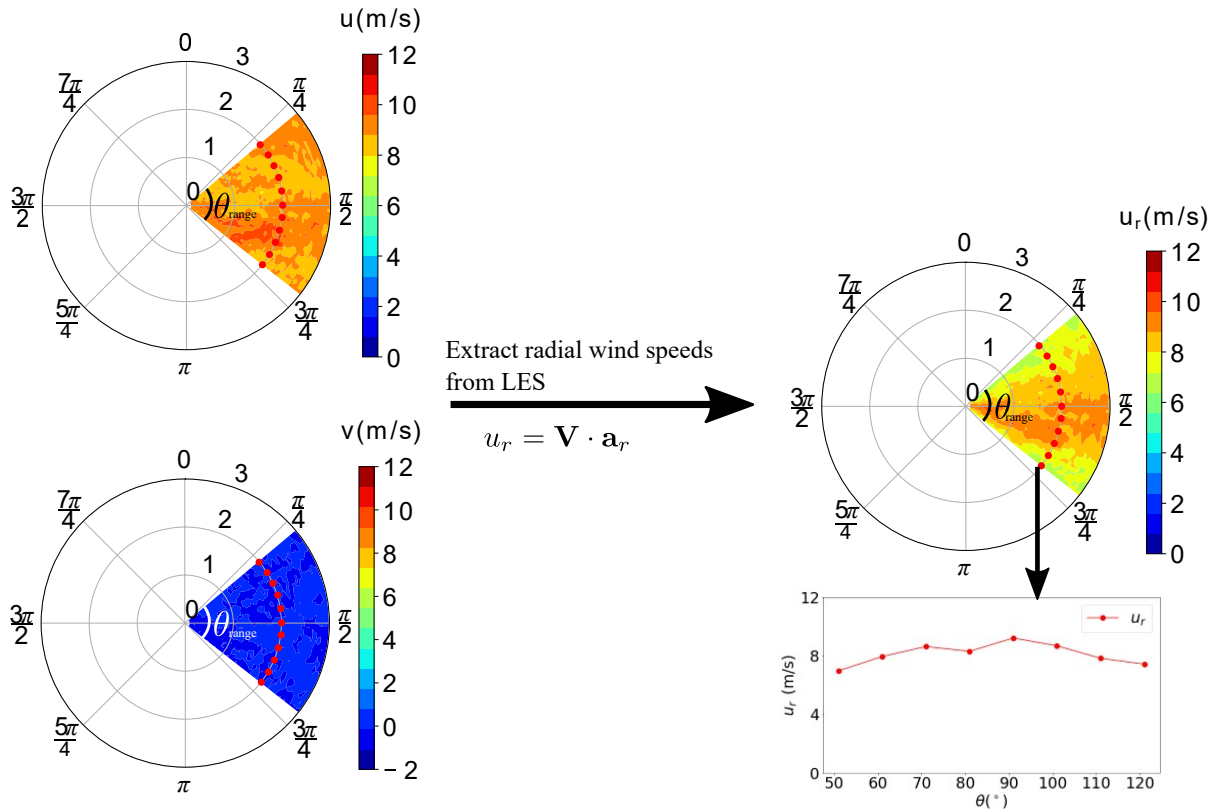
Figure A2. The method for extracting radial wind speed from the LES using Eq. (3) for a horizontal scan at a certain measurement range. The red dots are the radial wind speeds to be extracted for each azimuth angle.

365 *Author contributions.* JPG and TK jointly conceptualized and defined the objective of this work. MT performed all the simulations. MT and JPG performed data analysis and visualization. JPG and MT wrote original draft with significant contributions and revisions from TK.

Competing interests. The authors have no competing interest to disclose.

Acknowledgements. The authors acknowledges support from Furukawa Technology Promotion Foundation (FY 2022). The computations were performed on Oakbridge-CX supercomputer system of The University of Tokyo.

References

370

Banta, R. M., Pichugina, Y. L., Brewer, W. A., Lundquist, J. K., Kelley, N. D., Sandberg, S. P., Alvarez, R. J., Hardesty, R. M., and Weick-mann, A. M.: 3D volumetric analysis of wind turbine wake properties in the atmosphere using high-resolution Doppler lidar, Journal of Atmospheric and Oceanic Technology, 32, 904–914, https://doi.org/10.1175/JTECH-D-14-00078.1, 2015.

Barthelmie, R. J., Wang, H., Doubrawa, P., and Pryor, S. C.: Best practice for measuring wind speeds and turbulence offshore through in-situ and remote sensing technologies, Tech. rep., Cornell University, Ithaca, https://doi.org/10.7298/X4QV3JGF, 2016.

375

Bauweraerts, P. and Meyers, J.: Reconstruction of turbulent flow fields from lidar measurements using large-eddy simulation, Journal of Fluid Mechanics, 906, A17, 2021.

Courtney, M., Wagner, R., Murthy, R. K., and Boquet, M.: Optimized lidar scanning patterns for reduced project uncertainty, in: Proceeding of EWEA2014, Barcelona, 2014.

380

Coutts, E., Oldroyd, A., Stein, D., Krishna Murthy, R., Akhoun, M., Espin, F., and Garcia, L. M. G.: Cost effective offshore wind measurement, in: EWEA Resource Assessment, pp. 1–15, Helsinki, Finland, 2015.

Easterbrook, C. C.: Estimating Horizontal Wind Fields by Two-dimensional Curve Fitting of Single Doppler Radar Measurements, Radar Meteorology Conference, pp. 214–219, 1975.

ESI: OpenFOAM, https://www.openfoam.com [Accessed: 20 Feb. 2023], 2022.

385

Frehlich, R.: Scanning doppler lidar for input into short-term wind power forecasts, Journal of Atmospheric and Oceanic Technology, 30, 230–244, 2013.

Goit, J. P. and Önder, A.: The effect of coastal terrain on nearshore offshore wind farms: A large-eddy simulation study, J. Renewable Sustainable Energy, 14, 043 304, https://doi.org/10.1063/5.0094476, 2022.

Goit, J. P., Yamaguchi, A., and Ishihara, T.: Measurement and Prediction of Wind Fields at an Offshore Site by Scanning Doppler LiDAR and WRF, Atmosphere, 11, 442, 2020.

390

Goit, J. P., Taguchi, M., Tatsuno, J., and Kameda, T.: Effect of averaging time windows on wind resource assessment of small wind turbines, Wind Energy, 25, 1222–1237, https://doi.org/10.1002/we.2723, 2022.

Holleman, I.: Quality control and verification of weather radar wind profiles, Journal of Atmospheric and Oceanic Technology, 22, 1541–1550, 2005.

395

Iungo, G. V. and Porté-Agel, F.: Volumetric lidar scanning of wind turbine wakes under convective and neutral atmospheric stability regimes, Journal of Atmospheric and Oceanic Technology, 31, 2035–2048, 2014.

Koscielny, A. J., Doviak, R. J., and Rabin, R.: Statistical considerations in the estimation of divergence from single-Doppler radar and application to prestorm boundary-layer observations, Journal of Applied Meteorology, 21, 197–210, 1982.

Mukha, T., Rezaeiravesh, S., and Liefvendahl, M.: A Library for Wall-modelled Large-eddy Simulation based on OpenFOAM Technology, Computer Physics Communications, 239, 204–224, 2019.

400

Munters, W., Meneveau, C., and Meyers, J.: Shifted periodic boundary conditions for simulations of wall-bounded turbulent flows, Physics of Fluids, 28, 025 112, 2016.

Newsom, R. K., Berg, L. K., Shaw, W. J., and Fischer, M. L.: Turbine-scale wind field measurements using dual-Doppler lidar, Wind Energy, 18, 219–235, 2015.

405

Nicoud, F. and Ducros, F.: Subgrid-scale Stress Modelling Based on the Square of the Velocity, Flow, Turbulence and Combustion, 62, 183–200, 1999.

Rahlves, C., Beyrich, F., and Raasch, S.: Scan strategies for wind profiling with Doppler lidar–an large-eddy simulation (LES)-based evaluation, Atmospheric Measurement Techniques, 15, 2839–2856, 2022.

Sanchez Gomez, M., Lundquist, J. K., Mirocha, J. D., Arthur, R. S., Muñoz-Esparza, D., and Robey, R.: Can lidars assess wind plant blockage in simple terrain? A WRF-LES study, Journal of Renewable and Sustainable Energy, 14, 063 303, https://doi.org/10.1063/5.0103668, 2022.

Sathe, A. and Mann, J.: A review of turbulence measurements using ground-based wind lidars, Atmospheric Measurement Techniques, 6, 3147–3167, https://doi.org/10.5194/amt-6-3147-2013, 2013.

Shenghui, Z., Ming, W., Lijun, W., Chang, Z., and Mingxu, Z.: Sensitivity analysis of the VVP wind retrieval method for single-doppler weather radars, Journal of Atmospheric and Oceanic Technology, 31, 1289–1300, 2014.

Shimada, S., Goit, J. P., Ohsawa, T., Kogaki, T., and Nakamura, S.: Coastal wind measurements using a single scanning LiDAR, Remote Sensing, 12, 1347, https://doi.org/10.3390/RS12081347, 2020.

Shimada, S., Kogaki, T., Konagaya, M., Mito, T., Araki, R., Ueda, Y., and Ohsawa, T.: Validation of near-shore wind measurements using a dual scanning light detection and ranging system, Wind Energy, pp. 1–18, https://doi.org/10.1002/we.2757, 2022.

Simon, E. and Courtney, M.: A comparison of sector-scan and dual doppler wind measurements at Høvsøre test station—one lidar or two, DTU Wind Energy. DTU Wind Energy E, 112, 2016.

Stawiarski, C., Träumner, K., Knigge, C., and Calhoun, R.: Scopes and challenges of dual-Doppler lidar wind measurements—An error analysis, Journal of Atmospheric and Oceanic Technology, 30, 2044–2062, 2013.

Stawiarski, C., Träumner, K., Kottmeier, C., Knigge, C., and Raasch, S.: Assessment of surface-layer coherent structure detection in dual-Doppler lidar data based on virtual measurements, Boundary-Layer Meteorology, 156, 371–393, 2015.

Stevens, R. J., Graham, J., and Meneveau, C.: A concurrent precursor inflow method for Large Eddy Simulations and applications to finite length wind farms, Renewable Energy, 68, 46–50, 2014.

Tennekes, H. and Lumley, J. L.: A first Course in Turbulence, The MIT Press, 1972.

Viselli, A., Filipelli, M., Pettigrew, N., Dagher, H., and Faessler, N.: Validation of the first LiDAR wind resource assessment buoy system offshore the Northeast Univted States, Wind Energy, 22, 1548–1562, https://doi.org/10.1016/j.seta.2020.100878, 2019.

Waldteufel, P. and Corbin, H.: On the Analysis of Single-Doppler Radar Data, Journal of Applied Meteorology, 18, 532–542, 1978.

Zendehbad, M., Chokani, N., and Abhari, R. S.: Volumetric Three-Dimensional Wind Measurement Using a Single Mobile-Based LiDAR, Journal of Solar Energy Engineering, 138, 011 003, https://doi.org/10.1115/1.4031946, 2015.